

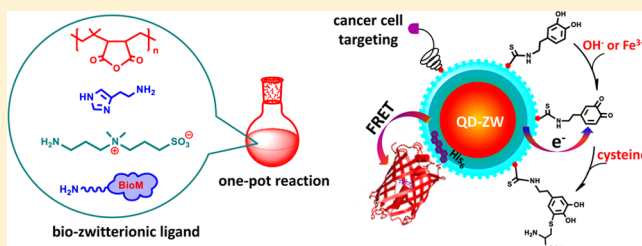
# A Multifunctional Polymer Combining the Imidazole and Zwitterion Motifs as a Biocompatible Compact Coating for Quantum Dots

Wentao Wang, Xin Ji, Anshika Kapur, Chengqi Zhang, and Hedi Mattoussi\*

Department of Chemistry and Biochemistry, Florida State University, 95 Chieftan Way, Tallahassee, Florida 32306, United States

**S** Supporting Information

**ABSTRACT:** We introduce a set of multicoordinating imidazole- and zwitterion-based ligands suited for surface functionalization of quantum dots (QDs). The polymeric ligands are built using a one-step nucleophilic addition reaction between poly(isobutylene-*alt*-maleic anhydride) and distinct amine-containing functionalities. This has allowed us to introduce several imidazole anchoring groups along the polymer chain for tight coordination to the QD surface and a controllable number of zwitterion moieties for water solubilization. It has also permitted the introduction of reactive and biomolecular groups for further conjugation and targeting. The QDs capped with these new ligands exhibit excellent long-term colloidal stability over a broad range of pH, toward excess electrolyte, in cell-growth media, and in the presence of natural reducing agents such as glutathione. These QDs are also resistant to the oxidizing agent H<sub>2</sub>O<sub>2</sub>. More importantly, by the use of zwitterion moieties as the hydrophilic block, this polymer design provides QDs with a thin coating and compact overall dimensions. These QDs are easily self-assembled with full size proteins expressed with a polyhistidine tag via metal–histidine coordination. Additionally, the incorporation of amine groups allows covalent coupling of the QDs to the neurotransmitter dopamine. This yields redox-active QD platforms that can be used to track pH changes and detect Fe ions and cysteine through charge-transfer interactions. Finally, we found that QDs cap-exchanged with folic acid-functionalized ligands could effectively target cancer cells, where folate-receptor-mediated endocytosis of QDs into living cells was time- and concentration-dependent.



## INTRODUCTION

Semiconductor nanocrystals, also called quantum dots (QDs), along with metal and metal oxide nanoparticles, possess unique size- and/or composition-tunable physical and spectroscopic properties.<sup>1–5</sup> For instance, QDs such as ZnS-overcoated CdSe nanocrystals exhibit narrow emission with high quantum yield and remarkable photostability.<sup>6–8</sup> Additionally, because these nanocrystals are in a size range comparable to those of biomolecules, they are very attractive for use as imaging probes and sensing and diagnostic tools.<sup>9–20</sup> Nonetheless, application of these materials in biology is still limited by constraints that include a rather large hydrodynamic size and limited colloidal stability.<sup>21–26</sup> The large size negatively affects their transport properties in biological media, such as cellular internalization, blood vasculature circulation lifetime, and renal clearance.<sup>21,22,25–27</sup> Furthermore, several important *in vivo* studies, such as fluorescence tracking of protein dynamics and detection of individual binding events, require the use of very low reagent concentrations.<sup>28</sup> However, achieving robust colloidal stability of hydrophilic QDs at nanomolar concentrations under ambient conditions is still challenging.<sup>23,24</sup> These properties are primarily dependent on the nature of the capping ligands and the surface coating strategy used to functionalize the nanocrystals.

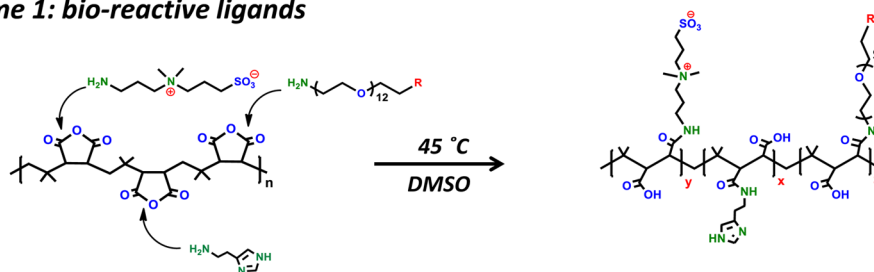
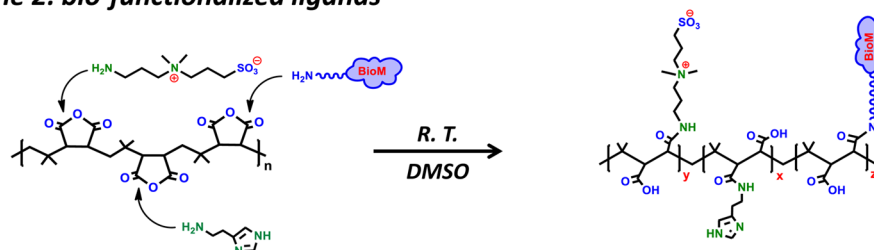
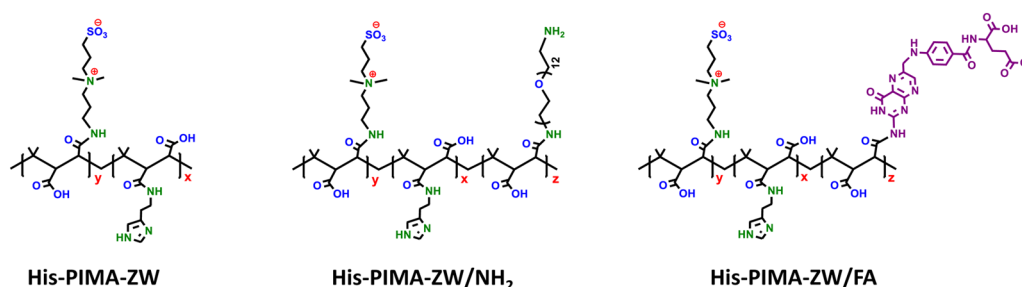
Water solubilization of high-quality QDs and other nanocrystals prepared using high-temperature growth routes has been achieved via either cap exchange with thiol-based metal-

coordinating ligands or encapsulation within amphiphilic block copolymers and phospholipid micelles.<sup>9,29–36</sup> However, both approaches face inherent limitations. For example, under room-temperature and light-exposure conditions, thiol-based ligands tend to oxidize with time, which can cause ligand desorption from the QD surface, resulting in aggregation; this is particularly important at very low reagent concentrations.<sup>23,37–39</sup> In addition, thiol coordination has been reported to weaken the QD fluorescence.<sup>40</sup> Conversely, the encapsulation strategy produces nanoparticles with limited stability at low concentrations and also tends to significantly increase the hydrodynamic radius of the QDs.<sup>34,41</sup>

Recently, several strategies have been explored to alleviate the above issues. To minimize the hydrodynamic size of the QDs without sacrificing aqueous solubility, a series of dihydroliipoic acid (DHLA)-based ligands appended with zwitterion groups have been developed as an alternative to poly(ethylene glycol) (PEG).<sup>24,42–47</sup> Because of their small volume, ligands based on the zwitterion motif yield nanocrystals with compact size. Additionally, imidazole-based ligands have been proposed by a few groups as an alternative to thiols because they are not affected by oxidation and tend to maintain high QD photoluminescence (PL).<sup>23,25,48,49</sup>

Received: August 22, 2015

Published: October 14, 2015

**Scheme 1: bio-reactive ligands****Scheme 2: bio-functionalized ligands****Representative ligands**

**Figure 1.** Schematic representation of the ligand synthesis using the one-step nucleophilic addition reaction starting with poly(isobutylene-*alt*-maleic anhydride): bio-reactive ligands (scheme 1) and ligands biofunctionalized in situ (scheme 2). Structures of three representative ligands are shown at the bottom: His-PIMA-ZW, His-PIMA-ZW/NH<sub>2</sub>, and the folic acid-modified ligand His-PIMA-ZW/FA.

In this study, a set of polyimidazole-based zwitterionic ligands have been developed to promote the phase transfer of hydrophobic QDs to aqueous media. This ligand design combines the benefits of the small-sized zwitterion with imidazole coordination. The ligand synthesis relies on a one-step nucleophilic addition reaction of distinct amine-containing functionalities with poly(isobutylene-*alt*-maleic anhydride) (PIMA). The resulting modular ligands have multiple imidazoles for metal coordination on the QD, several zwitterion moieties for water solubilization, and reactive groups for bioconjugation, as shown in Figure 1. In particular, this synthetic route allows the insertion of target biomolecules in situ during the ligand synthesis, thus integrating hydrophilic modification and bioconjugation of the QDs in one step (e.g., scheme 2 in Figure 1).

Functionalizing the QDs with these ligands produces dispersions that are highly fluorescent and exhibit long-term stability over a broad range of conditions, including in growth media, in the presence of oxidizing agents, and during storage at nanomolar concentrations under room-temperature and light-exposure conditions. Substituting PEG with zwitterion moieties produces QDs that are compact and easily conjugated with His-tagged proteins.<sup>50–54</sup> Additionally, covalent attachment of the neurotransmitter dopamine to QDs capped with amine-

modified polymer ligands provides a platform that can be used to sense pH changes, iron ions, and the amino acid cysteine via charge-transfer interactions. Finally, we show that folic acid-modified ligands can promote the delivery of large amounts of QDs into living cells through folate-receptor-mediated endocytosis.

## RESULTS AND DISCUSSION

**Ligand Design.** The present ligand design builds on previous ideas exploiting the highly efficient and specific nucleophilic addition reaction of maleic anhydride with amine-presenting molecules/moieties.<sup>31,35,39,55</sup> For example, we have applied this route, starting with PIMA, to prepare a few PEG-modified metal-coordinating ligands for the surface functionalization of QDs or Fe<sub>3</sub>O<sub>4</sub> nanoparticles.<sup>39,55</sup> In the present work, we have extended those rationales to prepare a set of hydrophilic, multicoordinating polymer ligands based on the zwitterion motif. The ability to carry out the synthesis without the need for coupling reagents or excess precursors eliminates constraints associated with compound purification because of the limited solubility of the zwitterion groups in organic solvents. In addition, this one-step reaction route is easy to implement compared with other polymer ligand designs, which

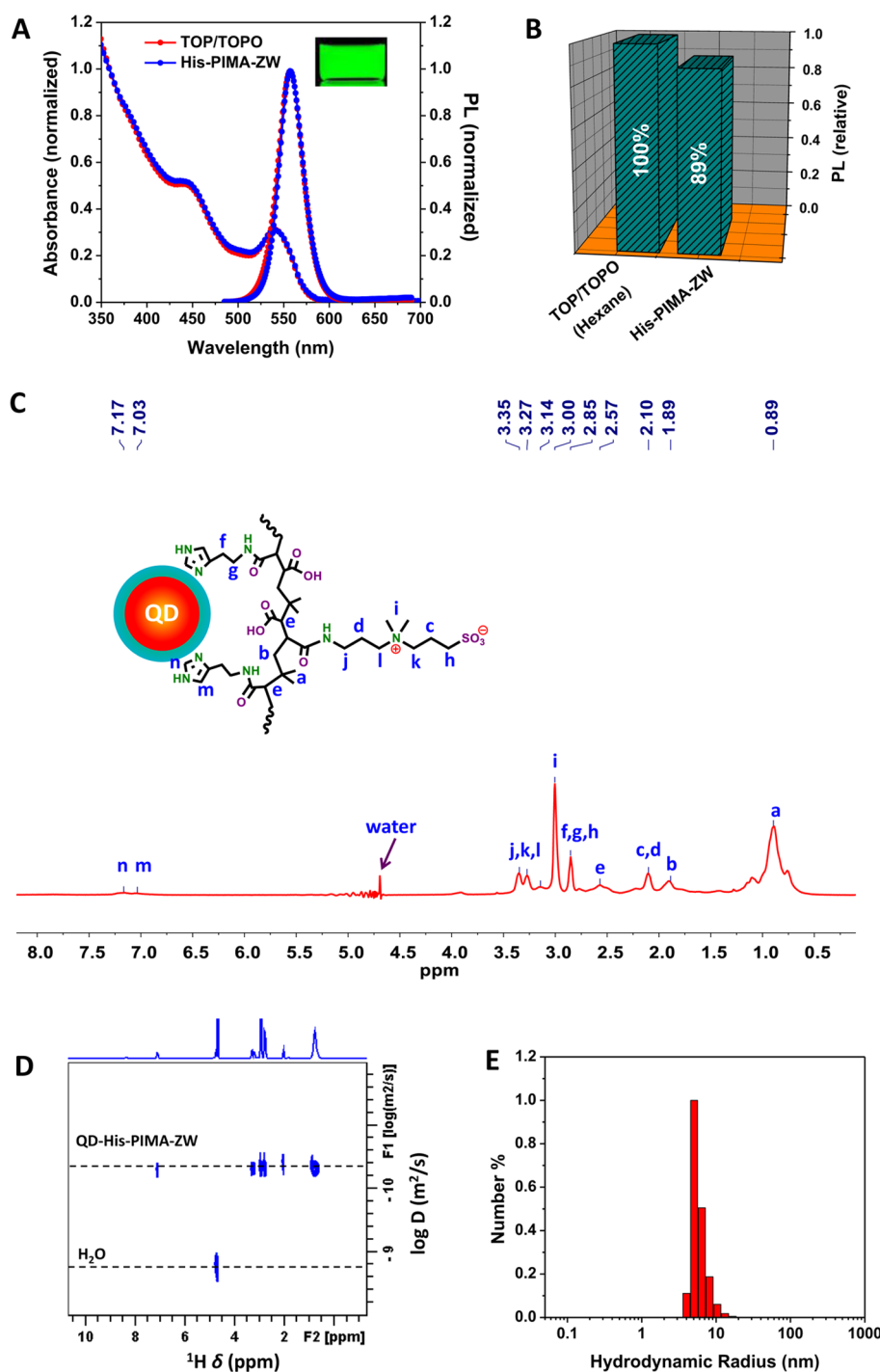


**Figure 2.** (A) Absorption and emission spectra of QDs (emitting at 556 nm) capped with TOP/TOPO in hexane (red line) and His-PIMA-ZW in H<sub>2</sub>O (blue line). The inset shows the fluorescence image of an aqueous QD dispersion (0.5 μM) irradiated using a hand-held UV lamp ( $\lambda_{\text{exc}} = 365$  nm). (B) PL intensity of His-PIMA-ZW-QDs in buffer (pH 7.5) relative to the intensity measured for the native QDs in hexane; the same optical density was used for both samples. (C) Pulsed-field-gradient-based water suppression <sup>1</sup>H NMR spectrum of hydrophilic QDs (in D<sub>2</sub>O); the assignment of the various peaks is detailed on the ligand structure. (D) DOSY spectrum collected from QDs capped with His-PIMA-ZW in D<sub>2</sub>O. (E) Histogram of the hydrodynamic size distribution measured for QDs capped with His-PIMA-ZW extracted from DLS measurements.

tend to require multistep syntheses with attendant purification requirements.<sup>23</sup>

Figure 1 summarizes the general schemes employed to prepare two sets of imidazole- and zwitterion-modified polymers: one set is made of bioreactive ligands, while the second is made of PIMA simultaneously coupled to zwitterion groups and biological receptors. (1) The bioreactive ligands are

polymers presenting zwitterion and reactive groups (e.g., carboxy, amine, and azide) along their backbones; the latter could be used for further coupling to target biomolecules. This set includes His-PIMA-ZW, made by reacting PIMA with a mixture of histamine (50%) and amino-zwitterion (50%). It is expected to introduce about 20 imidazole anchors and 20 zwitterion moieties while freeing ~40 reactive carboxylic groups

per PIMA chain. These carboxylic groups can be used for conjugation of the polymer-coated QDs to biomolecules, such as transferrin via 1-ethyl-3-(3-dimethylaminopropyl)-carbodiimide (EDC)/*N*-hydroxysuccinimide (NHS) chemistry. Another representative ligand, His-PIMA-ZW/R (R = amine, azide, biotin), is made from a stoichiometric mixture of histamine, amino-zwitterion, and reactive groups. This can be achieved by replacing a fraction of the amino-zwitterion moieties with H<sub>2</sub>N-PEG-R during the addition reaction. For example, we have prepared His-PIMA-ZW/NH<sub>2</sub> ligands in which the PIMA was modified with 10% H<sub>2</sub>N-PEG-NH<sub>2</sub> together with 40% amino-zwitterion and 50% histamine. (2) The biofunctionalized ligands are prepared by introducing amine-presenting biomolecules along with histamine and amino-zwitterion onto the PIMA chain during the nucleophilic addition reaction. We have synthesized the ligand His-PIMA-ZW/FA modified with 10% folic acid (along with 50% histamine and 40% amino-zwitterion) as a coating with potential cancer cell targeting capacity. Indeed QDs functionalized with His-PIMA-ZW/FA have been employed to target and deliver large amounts of QDs into living cells (see below). We should note that this scheme could in principle be used to introduce an array of amine-rich biomolecules into the polymer ligand, such as amine-terminated peptides or proteins.

**Ligand Exchange and Characterization of the Hydrophilic QDs.** To circumvent the limited solubility of zwitterion groups in commonly used organic solvents, the ligands (e.g., His-PIMA-ZW) were dissolved in small amounts of dimethyl sulfoxide (DMSO) prior to mixing with the hydrophobic QDs dispersed in chloroform. The mixture was left to stir at room temperature overnight. The displaced native ligands ( trioctylphosphine (TOP)/trioctylphosphine oxide (TOPO) and such) were then removed by two rounds of precipitation using a mixture of hexane and acetone followed by centrifugation. After gentle drying, the QD pellet was readily dispersed in buffer. Further purification of the QD dispersion was carried out using two rounds of concentration/dilution with deionized (DI) water using a centrifugal filtration device, yielding a clear and homogeneous colloidal suspension of nanocrystals. The hydrophilic QDs ligated with His-PIMA-ZW were characterized by optical spectroscopy, <sup>1</sup>H and <sup>31</sup>P NMR spectroscopy, diffusion-ordered spectroscopy (DOSY), and dynamic light scattering (DLS). The <sup>1</sup>H NMR data were further exploited to extract an estimate of the ligand density on the QD surface.

**1. Optical Characterization.** Figure 2A shows the absorption and emission spectra of a representative set of green-emitting QDs (emission peak at 556 nm) before and after ligand exchange with His-PIMA-ZW. The spectra of the hydrophilic QDs exhibit profiles identical to those collected for the starting materials (TOP/TOPO-capped), indicating that the integrity of the nanocrystals following phase transfer was maintained. The quantum yield (QY) of the QDs after ligand exchange was evaluated by comparing the PL of water-dispersible QDs to that of the hydrophobic ones dispersed in hexane. The relative PL intensity of the aqueous QDs with respect to the hydrophobic dispersion was ~90% (see Figure 2B). This rather high PL of the hydrophilic QDs derives from the benefits of imidazole coordination onto the QD surfaces;<sup>39</sup> it confirms and complements prior observations where conjugation of poly-histidine-tagged proteins onto DHLA-capped QDs produced a sizable enhancement in the PL signal.<sup>51,52</sup> Additional data on the optical characterization of other QD samples ligated with His-

PIMA-ZW and His-PIMA-ZW/FA are provided in Figure S2 in the Supporting Information.

**2. NMR Characterization.** The <sup>1</sup>H NMR spectrum collected from His-PIMA-ZW-QDs (Figure 2C) shows two distinct peaks at 7.03 and 7.17 ppm characteristic of the two protons in the imidazole ring; these peaks are slightly shifted and have lower intensity compared with those measured for the pure ligand as a result of the change in environment following coordination to the QD surface.<sup>39</sup> The pronounced resonance at 3.00 ppm corresponds to the methyl groups of the zwitterion moieties, while the smaller peaks at 2.10, 2.85, 3.27, and 3.35 ppm are ascribed to the CH<sub>2</sub> protons of the zwitterion and imidazole moieties (see Figure 2C). The broad peak at ~0.89 ppm is ascribed to the methyl protons in the PIMA chain. Similarly, the <sup>31</sup>P NMR spectrum collected from a dispersion of His-PIMA-ZW-QDs shows that the two sharp peaks at around -30 and 50 ppm and the weak peak at around 37 ppm, measured for the hydrophobic QDs and attributed to TOP, TOPO, and hexylphosphonic acid (HPA), respectively, disappeared following ligand exchange (see Figure S3). These data indicate that cap exchange with His-PIMA-ZW is highly efficient and is driven by the coordination of the imidazole groups to the QDs. Additional <sup>1</sup>H NMR data for QDs ligated with His-PIMA-ZW/FA are shown in Figure S4.

**3. Diffusion-Ordered Spectroscopy and Dynamic Light Scattering.** DOSY is a versatile, nondestructive technique that can resolve the diffusion coefficient, *D*, of subnanometer objects in solution, which makes it more suitable than DLS for characterizing rather small nanoparticles. It exploits the time-dependent signature of NMR-active atoms (e.g., <sup>1</sup>H, <sup>13</sup>C, <sup>31</sup>P) in a molecule of interest dispersed in a deuterated solution.<sup>57</sup> When applied to colloidal nanocrystals, DOSY provides a measure of the diffusion coefficients of ligands (associated with the observed resonances), thereby permitting the assignment of spectral features in the measured <sup>1</sup>H NMR spectrum to diffusing species that are either bound on the nanocrystals or free in the medium. For QDs ligated with His-PIMA-ZW, the various resonances in its <sup>1</sup>H NMR spectrum can be ascribed to two distinct diffusion coefficients (see Figure 2D). The faster diffusion (*D* = 1.78 × 10<sup>-9</sup> m<sup>2</sup>/s) is attributed to solubilized water molecules in the sample, while the slower diffusion (*D* = 4.16 × 10<sup>-11</sup> m<sup>2</sup>/s), which is associated with multiple proton resonances in the ligands, corresponds to His-PIMA-ZW-QDs (i.e., bound ligands). The absence of signals corresponding to unbound ligands in the measured spectrum indicates that following phase transfer and purification no measurable free ligands were left in the medium, further confirming the effectiveness of the ligand design and protocols used. A QD hydrodynamic radius (*R<sub>H</sub>*) of ~5.2 nm was extracted from the diffusion coefficient using the Stokes–Einstein equation:  $D = k_B T / (6\pi\eta R_H)$ , where *k<sub>B</sub>* is the Boltzmann constant, *T* is the absolute temperature (293 K), and *η* is the dynamic viscosity of the medium (~1 cP or 1.002 × 10<sup>-3</sup> N s/m<sup>2</sup>).<sup>58,59</sup> This value is in good agreement with the size extracted from DLS measurements (*R<sub>H</sub>* ≈ 5.7 nm) using the Laplace transform of the autocorrelation function (see Figure 2E). This size is comparable to that measured for DHLA-QDs. However, it is smaller than the values measured for DHLA-PEG<sub>750</sub>-QDs and for LA/His-PIMA-PEG-QDs with similar core radius: *R<sub>H</sub>* ≈ 8 nm for DHLA-PEG<sub>750</sub>-QDs and *R<sub>H</sub>* ≈ 11 nm for LA/His-PIMA-PEG-QDs.<sup>39,60</sup> The rather compact size offered by this polymer coating results from the combination of multicoordination on the QDs and the use of the zwitterion motif, yielding



homogeneous QDs with a very thin surface coating. Such a thin coating was further confirmed by the ability to conjugate polyhistidine-tagged proteins onto these QDs (see below).

**4. Estimation of the Ligand Density per QD.** The above NMR data were exploited to extract an estimate of the density of polymer ligands on the nanocrystals by comparing the total concentration of ligands with that of the QDs in the sample with added pyridine as a standard. The concentration of ligands was extracted by comparing the integrations of the methyl proton in the polymer backbone to the  $\alpha$ -proton in pyridine. The QD concentration was estimated from the absorbance at 350 nm.<sup>7</sup> This analysis yielded a value of  $\sim 13.3$  polymer ligands per QD emitting at 537 nm (radius of  $\sim 3.0$  nm, extracted from X-ray scattering).<sup>7,61</sup> This corresponds to  $\sim 260$  imidazole anchoring groups per QD. We also used NMR data to estimate the number of amines and folic acid groups per nanocrystal for QDs ligated with His-PIMA-ZW/NH<sub>2</sub> (10% amine) or His-PIMA-ZW/FA (10% folic acid). Overall, there were  $\sim 52$  amines or folic acid groups per QD. Additional details about the ligand density estimates using <sup>1</sup>H NMR data are provided in Figure S5.

**Colloidal Stability Tests.** The colloidal stability of aqueous QDs capped with His-PIMA-ZW was evaluated under several biologically relevant conditions, including a pH range of 3–13, high-ionic-strength buffers (1 M NaCl), growth media (100% RPMI-1640), and storage of nanomolar dispersions (e.g., 10 nM) under room-temperature and light-exposure conditions. Figure 3A shows fluorescence images of green-emitting QDs dispersed in buffers at pH 5–13 and in 1 M NaCl buffer, stored

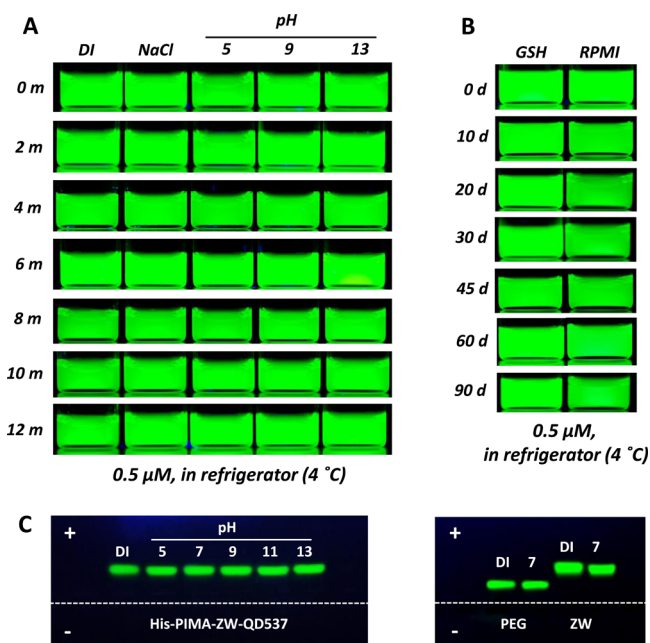


**Figure 3.** (A) Colloidal stability tests of QDs ligated with His-PIMA-ZW dispersed in DI water, NaCl solution (1 M), and phosphate buffer (20 mM) at different pH (5–13) over 12 months of storage. (B) Stability tests (over 3 months of storage) of QD dispersions in the presence of 10 mM glutathione (GSH) and when mixed with RPMI-1640 growth medium. The concentration of QDs was  $\sim 0.5 \mu\text{M}$ . All of the samples were stored at 4 °C. (C) Agarose gel electrophoresis images of QDs ligated with His-PIMA-ZW at different pH from 5 to 13 (left) side-by-side with images of QDs ligated with LA/His-PIMA-PEG (described in ref 39) dispersed in DI water and in pH 7 buffer (right). The concentration of QDs was  $\sim 0.5 \mu\text{M}$ . The dashed line indicates the location of the loading wells.

at  $\sim 4$  °C in the dark. All of the QD dispersions stayed stable for at least 12 months with no sign of aggregation or loss of fluorescence. Additional data on the stability of QDs in pH 3 buffer are provided in Figure S6, where His-PIMA-ZW-QDs stayed stable for at least 5 weeks, although the fluorescence decreased after 3 weeks. This reduced stability at such low pH is expected because of protonation of the imidazole groups ( $\text{p}K_{\text{a}} \approx 6.0$  for imidazole).<sup>62</sup> Similar observations have been reported for other imidazole-based ligands at  $\text{pH} \leq 5$ .<sup>23,48</sup> For example, we have found that the dispersion of QDs coated with His-PIMA-PEG (PEGylated polymer) exhibit a progressive loss in the measured fluorescence at pH 3 after 1 month of storage; nonetheless, the photostability can be substantially improved by using mixed coordination ligands (LA/His-PIMA-PEG).<sup>39</sup> The colloidal stability of QDs was further assessed in the presence of endogenous thiols (i.e., glutathione) and in cell-growth media. The fluorescence images of QD dispersions in 10 mM glutathione solution and 100% RPMI-1640 growth medium (Figure 3B) show no aggregation buildup or loss of fluorescence over 3 months of storage. The above results are very important for the use of such QDs to investigate intracellular media, which are rich in ions, proteins, and reducing agents.

We complemented the above results by carrying out gel electrophoresis measurements of hydrophilic QDs to determine whether pH changes can affect the QD mobility and whether the zwitterion coating provides net charges to the QD surface in addition to those provided by the carboxy groups on the polymer backbone. Figure 3C shows that the fluorescent bands of the His-PIMA-ZW-QDs at pH 5–13 are narrow (with no observable smearing) with essentially identical mobility shifts. In comparison, the bands measured for QDs coated with PEGylated polymer (i.e., LA/His-PIMA-PEG-QDs) are also narrow but have smaller mobility shifts than those measured for the His-PIMA-ZW-QDs (see Figure 3C). These results indicate that the dispersions are made with uniform distributions of nanocrystal size and surface charge density across the pH range. They also imply that the zwitterion groups provide a net negative charge to the QDs in addition to those provided by the carboxy groups. Furthermore, the density of surface charges for each coating is not affected by pH changes, as reflected by the identical mobility shifts measured at various pH values, although larger shifts were measured for the zwitterionic coating.<sup>39</sup> Previous reports have also shown that zwitterion moieties contribute a net negative charge attributed to the strong ionic signature of the sulfobetaine groups.<sup>43,44</sup>

We further tested the colloidal stability of His-PIMA-ZW-QDs at low concentrations and under room-temperature and light-exposure conditions. The fluorescence images in Figure 4A indicate that the QDs stayed stable for at least 4 months at all the concentrations used (300, 50, and 10 nM). The PL intensity measured for the 300 nM QD dispersion was essentially unchanged for at least 60 days. For the 50 nM and 10 nM dispersions, the fluorescence emission was maintained for the first month but gradually decreased after that. For example, losses of  $\sim 30\%$  and  $\sim 50\%$  were measured for the 50 nM and 10 nM dispersions, respectively, after 2 months (Figure 4B). In comparison, a pronounced reduction in the PL was measured for QDs photoligated with LA-PEG<sub>750</sub>-OME-QDs, as reported in ref 44. The reduced stability of QDs capped with molecular thiol derivatives at low concentrations over time has been attributed to possible thiol oxidation and ligand desorption from the QD surfaces.<sup>23,38,39</sup> Stability against oxidation was monitored for our newly capped QDs when they were dispersed

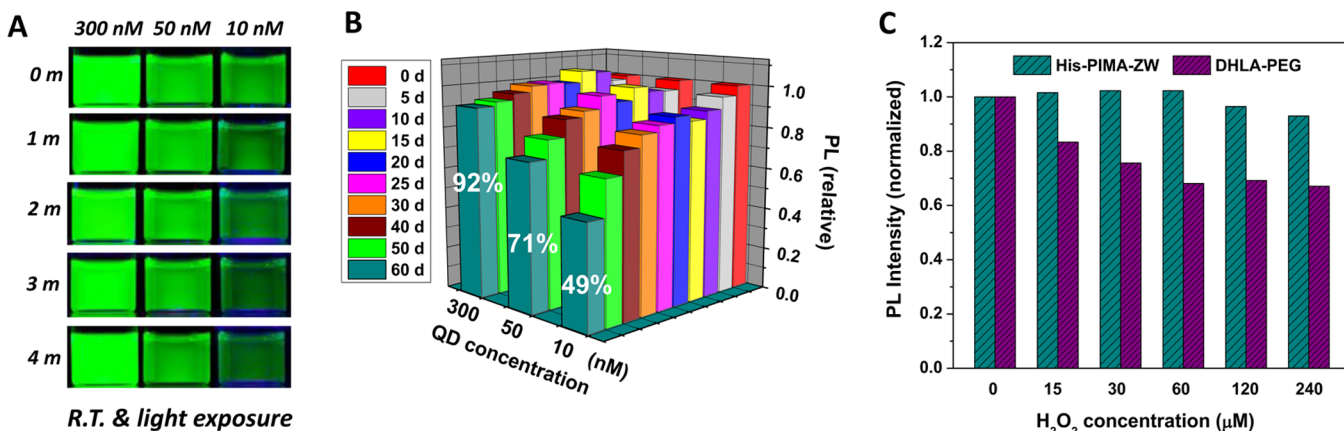


**Figure 4.** (A) Fluorescence images of three sets of QD dispersions during storage at room temperature and under light exposure for up to 4 months. The concentrations were 300, 50, and 10 nM, respectively. (B) Time progression of the PL intensities of these three QD samples normalized with respect to the value measured on day 0. (C) Normalized PL intensities of His-PIMA-ZW-QDs and DHLLA-PEG-QDs against chemical oxidation in the presence of increasing concentrations of H<sub>2</sub>O<sub>2</sub>.

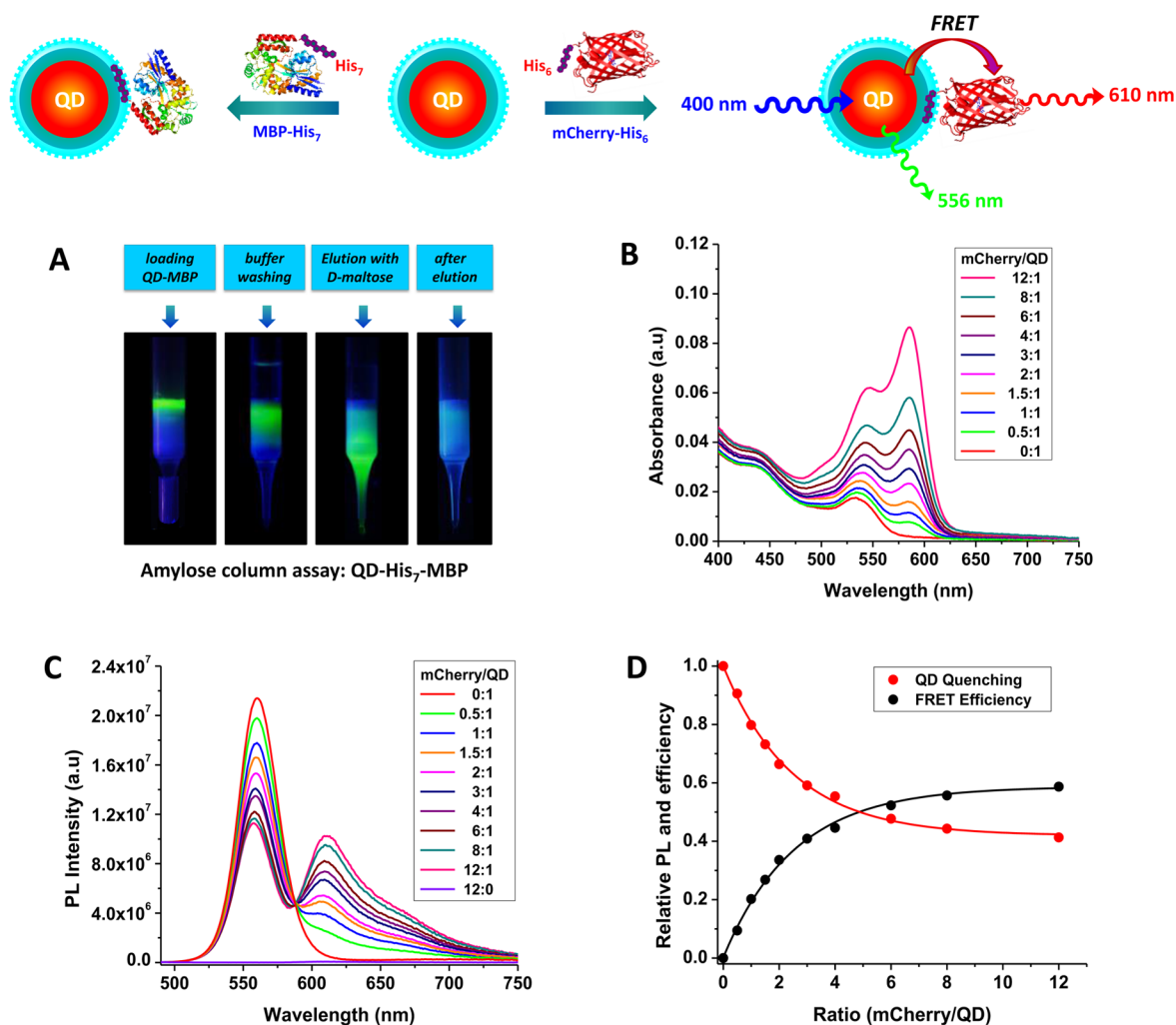


**Figure 5.** (top) Schematic representation of the bioconjugation between His-PIMA-ZW-QDs and proteins driven by polyhistidine coordination. (A) Amylose chromatography assay testing conjugation of QDs with MBP-His<sub>7</sub>. The MBP:QD ratio was 12:1. (B, C) Evolution of the absorption and emission spectra of QD–mCherry-His<sub>6</sub> conjugates as a function of the protein:QD ratio (valence), which was varied between 0:1 and 12:1. (D) Experimental values of the relative QD PL decay (red circles) vs valence  $n$  together with the corresponding FRET efficiencies (black circles) with a fit to a hyperbolic function of the form  $E = nR_0^6 / (nR_0^6 + r^6)$ . Additional details on the FRET analysis are provided in the [Supporting Information](#).

in a solution of hydrogen peroxide. [Figure 4C](#) shows that the QD PL was essentially unaffected by the addition of H<sub>2</sub>O<sub>2</sub>

throughout the range of concentrations tested up to 240 μM, with the PL intensity remaining at 95%–100% of its initial value.

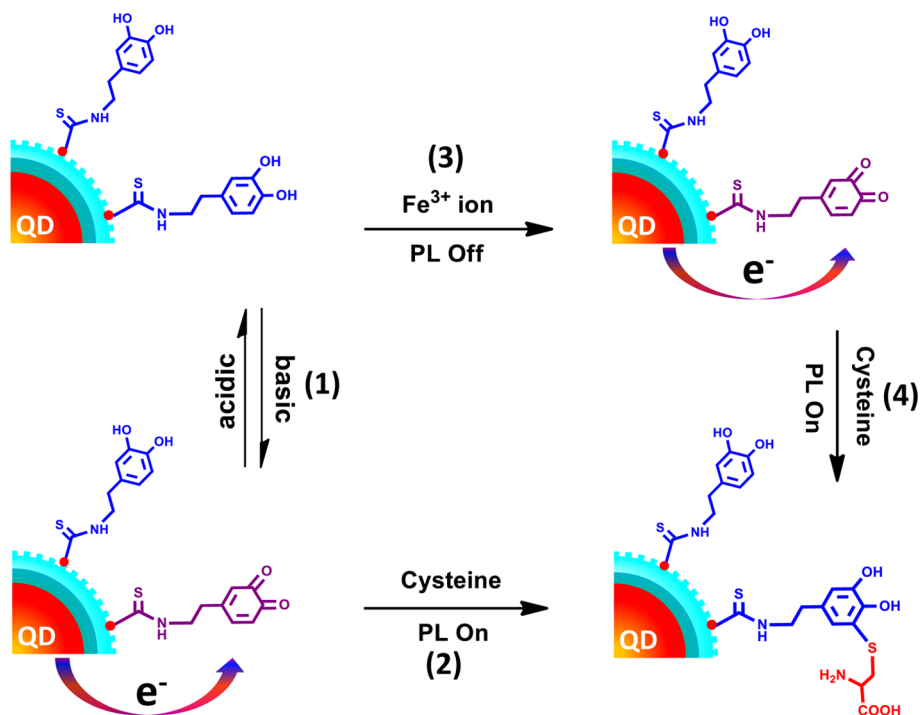


**Figure 6.** Schematic representation of the changes in the charge-transfer interactions between QDs and proximal dopamine as a function of pH, added cysteine, or added iron ions.

In comparison, DHLA-PEG<sub>750</sub>-OMe-QDs exhibited weaker resistance to H<sub>2</sub>O<sub>2</sub>, as indicated by a ~30% reduction in PL measured at 60–240 μM H<sub>2</sub>O<sub>2</sub>.

Overall, the better colloidal stability at pH 5–13, toward H<sub>2</sub>O<sub>2</sub> oxidation, and in growth media proves the great tolerance of the His-PIMA-ZW-QDs to photo- and chemical oxidation, a result that can be attributed to the enhanced coordination of multiple imidazole ligands and the strong affinity of the zwitterion moieties for water.

**QD–Protein Conjugation.** Direct immobilization of polyhistidine-appended biomolecules onto the nanocrystal surface as a means of forming QD–bioconjugates driven by metal-affinity coordination has been applied to attach peptides and proteins to core–shell QDs and gold nanoparticles (AuNPs) alike.<sup>50,51,53,54,63</sup> This is an attractive route because of its ease of implementation and the ubiquitous presence of His-tagged proteins expressed in bacteria or synthetically prepared peptides. However, one key requirement for such conjugation is the use of small capping ligands so that the His tag is able to directly reach the nanocrystal surface. In our previous work, DHLA-capped QDs have been extensively used for conjugation with His-tagged proteins, but the colloidal stability of these nanocrystals was limited to basic conditions.<sup>51–53</sup> Here we applied this conjugation strategy to the His-PIMA-ZW-capped QDs (emitting at 556 nm) using two proteins: maltose binding protein (MBP) appended with a N-terminal seven-histidine tag (MBP-His<sub>7</sub>) and a fluorescent protein (mCherry) appended with a N-terminal six-histidine tag (mCherry-His<sub>6</sub>).

**1. QD–MBP Conjugates: Amylose Column Assay.** QD–MBP conjugation was tested using amylose chromatography followed by competitive release with maltose (see Figure 5). Following incubation of MBP-His<sub>7</sub> with His-PIMA-ZW-QDs (MBP:QD ratio = 12:1), the resulting QD–MBP conjugates were tightly bound onto the top of the amylose column (as

indicated by the green fluorescence band observed under irradiation using a hand-held UV lamp) and were not eluted even after three washes with buffer; this binding is promoted by the affinity of MBP to the amylose gel. Addition of 1 mL of 20 mM D-maltose, the substrate of MBP, readily resulted in elution of the conjugates. Binding to amylose and release by addition of maltose, complemented with the fluorescence emission of the band, confirmed that the conjugation between MBP-His<sub>7</sub> and the polymer-capped QDs took place. We should note that conjugation of DHLA-QDs to His-tagged proteins has been accompanied by an enhancement of the QD emission.<sup>51,52</sup> A similar trend was observed for our conjugates, with a progressive increase in the sample PL as the MBP:QD ratio increased from 0:1 to 12:1 (see Figure S7). However, this enhancement was much smaller than that measured for MBP-His<sub>5</sub> self-assembled onto DHLA-capped QDs.<sup>51,52</sup> For instance, an enhancement of only ~20% was measured for the His-PIMA-ZW-QDs conjugated with approximately eight MBP-His<sub>7</sub>, while an increase of ~90% was measured for DHLA-QDs with the same conjugate valence.<sup>52</sup> Such a variance is likely due to the different natures of the surface capping ligands. Thiol-appended ligands tend to lower QD PL, and hence, the effects of polyhistidine tag coordination are more pronounced.<sup>40</sup> In contrast, His-PIMA-ZW-QDs already have high PL signal with multi-imidazole coordination, limiting the enhancement effects of His-tagged protein conjugation.

**2. QD–mCherry Conjugates: FRET Analysis.** Self-assembly of the fluorescent mCherry protein appended with a His<sub>6</sub> tag onto His-PIMA-ZW-QDs was verified by evaluating the fluorescence resonance energy transfer (FRET) interactions. Figure 5B shows the absorption spectra of QD–mCherry-His<sub>6</sub> at a protein:QD ratio (conjugate valence) ranging from 0:1 to 12:1. The progressive increase in the absorption peak at ~586 nm is due to the mCherry contribution. The corresponding composite emission spectra, collected using excitation at 400

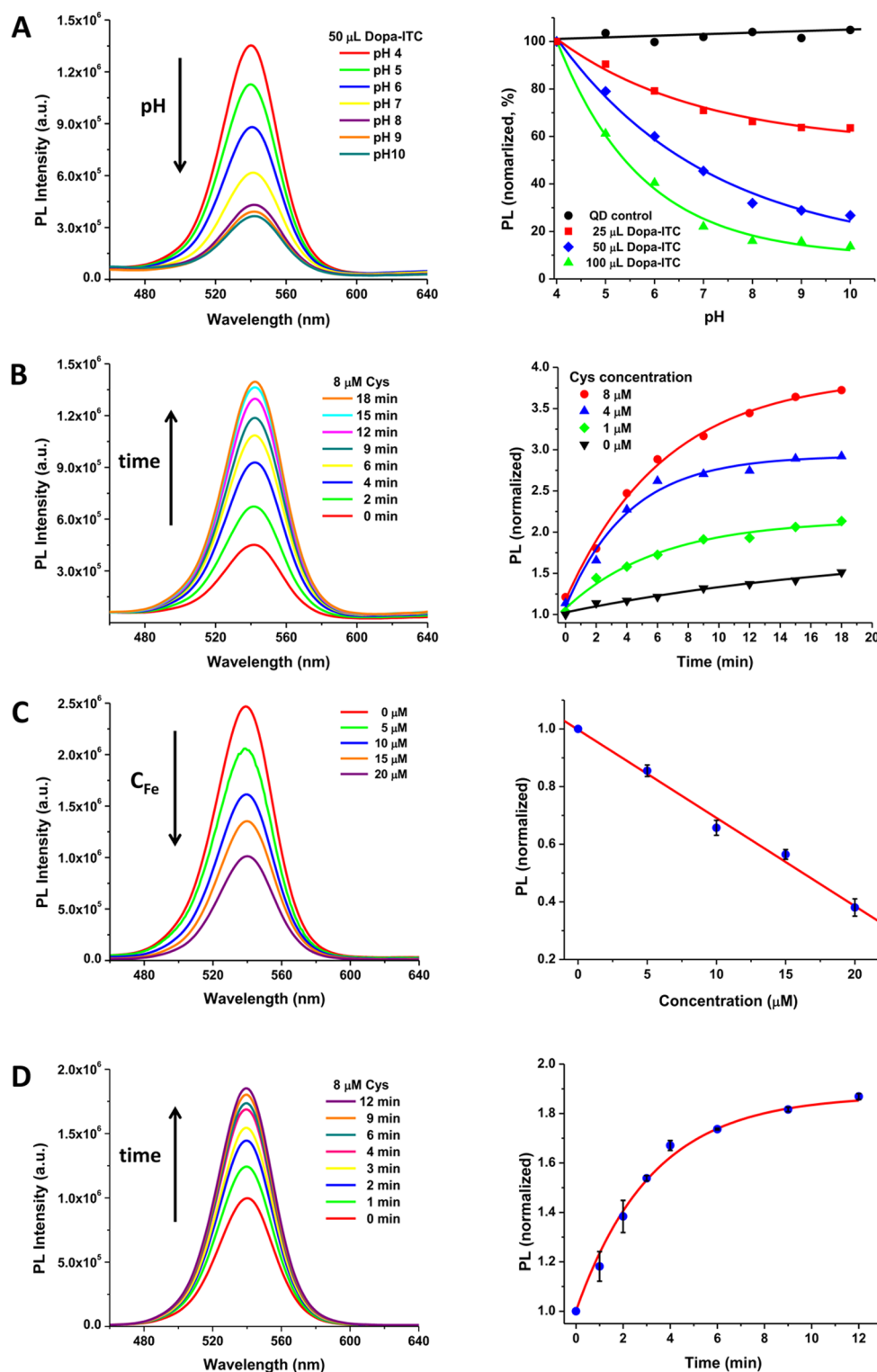


**Figure 7.** (A) PL spectra collected from dispersions of QD–dopamine conjugates at pH from 4 to 10, together with the integrated PL intensity normalized with respect to the value at pH 4. The PL spectra (left) were collected from conjugates prepared using 50  $\mu\text{L}$  of dopamine-ITC (see the Experimental Section). (B) Time progression of the PL spectra of QD–dopamine conjugates (initially dispersed at pH 10) mixed with 8  $\mu\text{M}$  cysteine. Also shown are plots of the integrated PL intensity with time for different concentrations of added cysteine. The PL is normalized with respect to the initial value at 0 min. (C) PL spectra of QD–dopamine conjugates (prepared using 25  $\mu\text{L}$  of dopamine-ITC) in the presence of different concentrations of Fe from 0 to 20  $\mu\text{M}$ , together with the integrated PL intensity normalized with respect to the value at 0  $\mu\text{M}$  Fe. (D) Time progression of the PL spectra of Fe-catalyzed QD–dopamine conjugates in the presence of 8  $\mu\text{M}$  cysteine, together with the integrated PL intensity normalized with respect to the value at 0 min.

nm, are shown in Figure 5C. The spectra show a progressive loss in QD emission accompanied by a gradual increase in mCherry

emission as the protein:QD molar ratio increases. Since the fluorescence due to direct excitation of mCherry is negligible



(see the violet profile in Figure 5C), we attribute the fluorescence contribution of mCherry in the composite spectra to FRET sensitization of the protein.

Values for the relative QD PL losses along with the FRET efficiencies, derived from the deconvoluted emission spectra as a function of conjugate valence, are shown in Figure 5D. The trends for both experimental parameters agree well with the predictions based on FRET interactions between one central donor and  $n$  equally spaced acceptors surrounding it. Using the expression for the FRET efficiency for the above conjugate configuration,  $E = nR_0^6/(nR_0^6 + r^6)$ , where  $R_0$  and  $r$  are the Förster radius and QD-to-mCherry center-to-center separation distance, respectively, we extracted an experimental estimate of  $\sim 60$  Å for  $r$ . This value is comparable to the value measured for mCherry-His<sub>6</sub> self-assembled onto QDs photoligated with bis(LA)-ZW ligands but slightly larger than the value reported for mCherry self-assembled onto green-emitting DHLA-QDs ( $r \approx 56$  Å).<sup>44,64</sup> Additional details of the FRET analysis along with the corresponding parameters are provided in Figure S8 and Table S1. We should note that in order to account for the small enhancement in QD PL upon conjugation to polyhistidine-tagged proteins, the PL from dispersions of QD-MBP-His<sub>7</sub> conjugates were used as control/reference samples to calculate the experimental FRET efficiencies. This result is greatly promising for the formation of self-assembled QD-protein conjugates, as control over the valence and potentially over the protein orientation is easily achieved using this approach.

**QD-Dopamine Conjugates as PL Sensing Platforms.** It has been reported that oxidized dopamine can interact with the cysteine residues of parkin, a ligase protein that mediates the degradation of proteins toxic to dopaminergic neurons.<sup>65</sup> This covalent modification results in degeneration of nigral neurons over time due to the inactivation of its ubiquitin ligase function. Meanwhile, the oxidative metabolism of dopamine has received a great deal of attention in Parkinson's disease because it yields quinones, hydrogen peroxide, and other reactive oxygen species (ROS), which could damage lipids, proteins, and DNA and consequently lead to cell death.<sup>66</sup> Those studies also indicate that oxidative metabolism of dopamine is closely related to iron catalysis and depletion of biothiols molecules (e.g., cysteine) to form 5-S-cysteinyl-dopamine.<sup>67–69</sup>

We tested some of these interactions by probing their effects on the fluorescence emission of QD-dopamine conjugates. For this we first reacted dopamine isothiocyanate (dopamine-ITC) with His-PIMA-ZW/NH<sub>2</sub>-capped QDs to promote covalent attachment via isothiourea bonds.<sup>70</sup> This produces sensing platforms where the fluorescence emission can be modulated by charge-transfer (CT) interactions between the QD and proximal dopamines.<sup>70</sup> We used these conjugates to probe changes in the buffer pH, the effects of added iron ions, and interactions with the amino acid cysteine. Figure 6 shows a schematic representation of the proposed modulation of the QD PL via four distinct pathways: (1) pH-induced PL changes attributed to a change in the oxidation potential of catechol with increasing pH combined with a shift in the chemical equilibrium between dopamine catechol (reduced form) and dopamine quinone (oxidized form).<sup>70</sup> (2) Interactions of QD-dopamine dispersed in pH 10 buffer with cysteine. Here the thiol group of cysteine reacts with quinone (dominant at pH 10) to form 5-S-cysteinyl-dopamine. This reaction produces recovery of the QD PL due to a reduction in the CT interactions with the QDs as the concentration of quinone in the medium is decreased. (3) Interactions of QD-dopamine with Fe ions in DI water, where

Fe-catalyzed oxidation of dopamine increases the concentration of quinone, thus enhancing electron-transfer interactions with the QDs. This results in pronounced PL loss that directly traces the concentration of added Fe ions. (4) Effects of competing interactions between cysteine and QD-dopamine premixed with Fe ions. The added cysteine molecules compete with Fe ions for interactions with quinone, promoting a reverse transformation to 5-S-cysteinyl-dopamine. This transformation alters the nature of the QD-dopamine interactions, resulting in recovery of the QD PL.

**1. pH-Dependent Quenching of QD Fluorescence.** Figure 7A shows the PL spectra collected for the set of QD-dopamine conjugates when the buffer pH was changed from 4 to 10; progressive quenching was observed as the pH was shifted from acidic to basic. These intermediate-valence conjugates were prepared using 50  $\mu$ L of dopamine-ITC during the coupling reaction (see the Experimental Section). Cumulative plots of the progression of the normalized PL with pH for all three sets of conjugates prepared with different dopamine:QD molar ratios are shown. Similar quenching behavior was measured for all three dispersions, although the quenching was more pronounced for samples prepared with higher conjugate valence. In comparison, no change in the QD PL was measured for the control sample made of QDs alone. These results are consistent with previous data obtained for QDs capped with DHLA-PEG ligands.<sup>70–72</sup> The progressive PL loss with increasing pH can be attributed to CT interactions between the QD and dopamine. Such interactions involve complex electron and hole exchange between photoexcited QDs and a mixture of the reduced (catechol) and oxidized (quinone) forms of dopamine.<sup>71,72</sup>

**2. Probing the Interactions between QD-Dopamine Conjugates and Cysteine.** We utilized the above QD-dopamine conjugates to probe interactions with cysteine; cysteine solution was added to a dispersion of QD-dopamine preset at pH 10. Figure 7B shows the changes in QD PL with reaction time when QD-dopamine conjugates were dispersed in the presence of 8  $\mu$ M cysteine. The QD PL exhibited a progressive increase with time until saturation was reached. Moreover, the normalized PL intensities at saturation were concentration-dependent. These results indicate that the transformation from quinone to 5-S-cysteinyl-dopamine was faster in the presence of higher concentrations of cysteine (faster reaction kinetics). Control experiments (QDs alone) showed marginal changes in PL signal. This indicates that our polymer-coated QDs are neither pH-sensitive nor affected by potential cysteine competition for surface coordination (see Figure S9).

**3. Sensing of Fe Ions with QD-Dopamine Conjugates.** Figure 7C shows the PL spectra together with a plot of the normalized PL data collected from dispersions of QD-dopamine conjugates mixed with varying concentrations of Fe ions ranging from 0 to 20  $\mu$ M. The QD-dopamine conjugates were prepared by reacting the polymer-coated QDs with 25  $\mu$ L of dopamine-ITC. A linear decrease in the PL was measured when the iron concentration was increased in the tested range (Figure 7C).

**4. Competitive Binding of Cysteine to Quinone.** Addition of cysteine to the above dispersions containing QD-dopamine conjugates premixed with Fe ions was found to induce a partial recovery of the QD PL, as shown in Figure 7D. This is attributed to competition between the cysteine and Fe ions for interaction with the conjugates, which induces a reverse transformation from quinone (produced by Fe catalysis) to 5-S-cysteinyl-dopamine. Nonetheless, the recovery is not full, as a fraction of

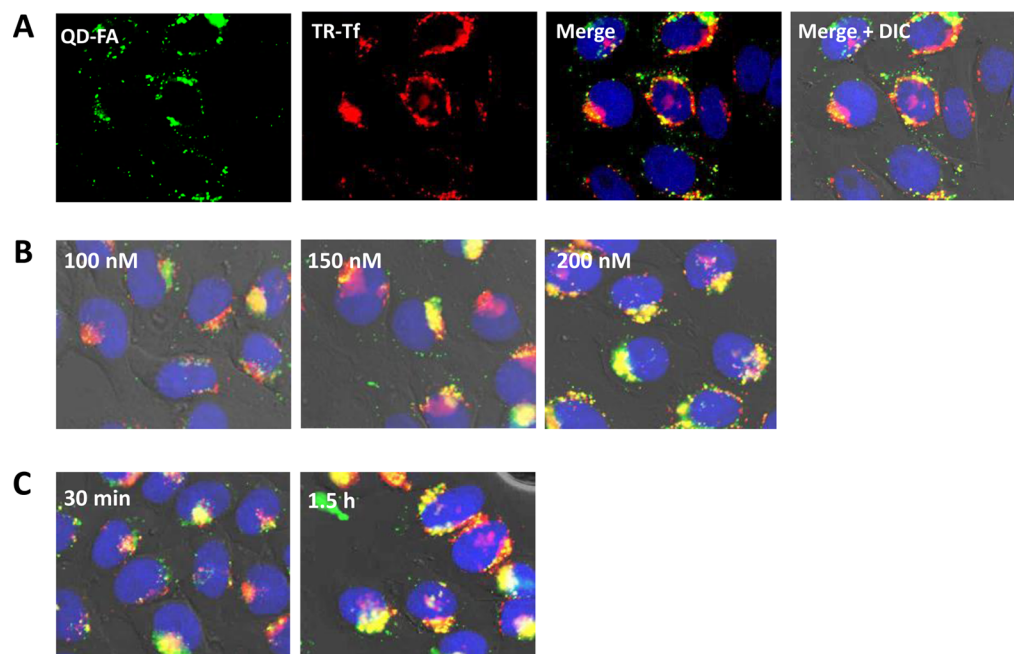


**Figure 8.** (A) Representative epifluorescence images collected from HeLa cells coincubated with 200 nM QD-FA and 0.5  $\mu\text{M}$  Texas Red-transferrin for 1 h. From left to right, the panels correspond to QD fluorescence (green,  $\sim 537$  nm), Texas Red-transferrin as an endosome-specific marker (red,  $\sim 615$  nm), and composite images with DAPI (blue,  $\sim 460$  nm) and differential interference contrast (DIC). (B) Concentration-dependent cellular internalization of QD-FA. The merged fluorescence images were collected for HeLa cells coincubated with 0.5  $\mu\text{M}$  Texas Red-transferrin and 537 nm-emitting QD-FA at different concentrations: (left) 100 nM, (middle) 150 nM, and (right) 200 nM. (C) Time-dependent intracellular uptake of QD-FA. The composite images were collected for HeLa cells coincubated with 200 nM QD-FA and 0.5  $\mu\text{M}$  Texas Red-transferrin for 30 min and 1.5 h.

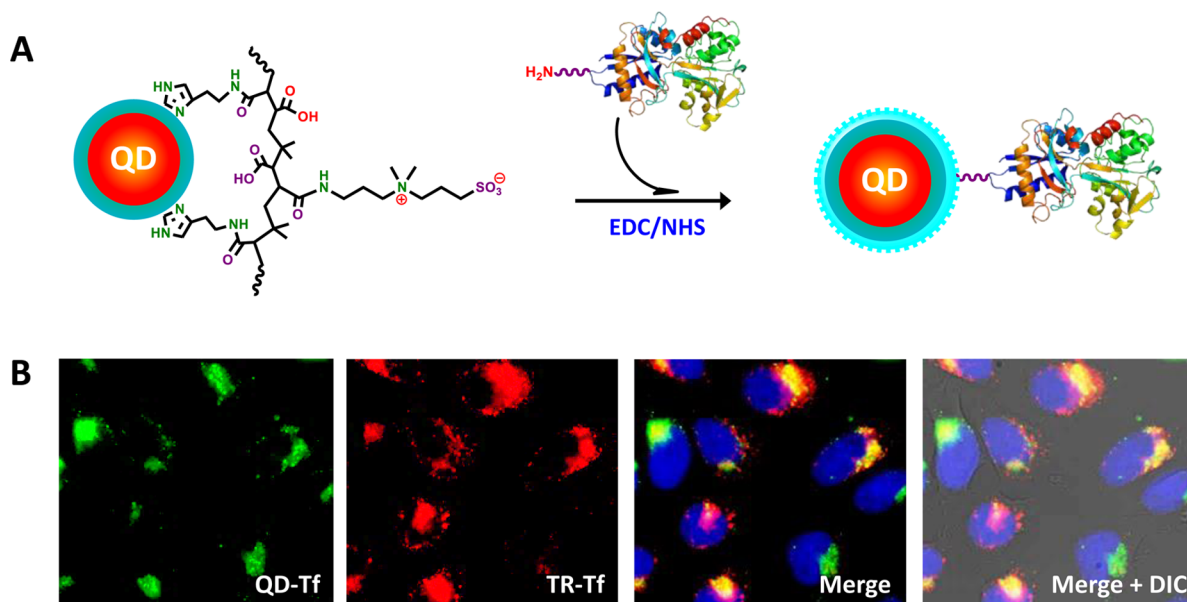


**Figure 9.** (A) Schematic of the assembly of QD-transferrin conjugates via EDC/NHS coupling. (B) Representative images of HeLa cells incubated with 200 nM QD-transferrin conjugates for 1 h and then with 0.5  $\mu\text{M}$  Texas Red-transferrin for 40 min. The QD fluorescence image (green), Texas Red-transferrin fluorescence image (red), and composite images with DAPI fluorescence (blue) and differential interference contrast (DIC) are shown from left to right.

the Fe and cysteine may still interact simultaneously with dopamine, forming 5-cysteinyldopamine-Fe complexes; this configuration would still produce partial quenching of the QD PL. Additional details about the CT interactions involved are provided in the [Figure S11](#).

**Intracellular Delivery of Folic Acid-Decorated QDs.** The folate receptor protein is a biomarker commonly

overexpressed on the membranes of breast, lung, kidney, and ovary epithelial cancer cells.<sup>73,74</sup> It has high affinity for folic acid (with a reported dissociation constant,  $K_D$ , of  $\sim 0.1$  nM) and promotes its intracellular transport via receptor-mediated endocytosis.<sup>73,75,76</sup> This uptake mechanism has been exploited to promote the intracellular uptake of folic acid-conjugated nanoparticles and drugs as well as for use in tumor-targeting,

imaging, and anticancer therapy.<sup>73,77,78</sup> Here we demonstrate that our folic acid-modified ligand (His-PIMA-ZW/FA) can promote the delivery of large amounts of QDs into live cells.

Figure 8A shows epifluorescence images collected for HeLa cells coincubated with QD-His-PIMA-ZW/FA (QD-FA, 200 nM) and Texas Red–transferrin (0.5  $\mu$ M) for 1 h. These images correspond to the QD emission (green), Texas Red–transferrin endolysosomal marker (red), a merged composite fluorescence image with 4',6-diamidino-2-phenylindole (DAPI) staining of the nuclei (blue), and a superposition of the fluorescence and differential interference contrast (DIC) images. The images show the presence of punctate QD fluorescence distributed in the perinuclear region, with no apparent nuclear staining. The QD fluorescence was mostly colocalized with the distribution of endo/lysosomal compartments, as shown in the merged images, indicating that the QD-FA conjugates have been mainly internalized via folate-mediated endocytosis. In comparison, control experiments carried out using cells incubated with QD-His-PIMA-ZW (no folic acid) showed no intracellular QD fluorescence (see Figure S12).

To probe the efficiency of folic acid-mediated internalization, we incubated cells with QD-FA conjugates at different concentrations and for different time intervals. Figure 8B shows three representative fluorescence images collected for HeLa cells incubated with 100, 150, or 200 nM QD-FA conjugates for 1 h. The images clearly show that the intracellular uptake of QDs was concentration-dependent, with the highest fluorescence observed for cells incubated with 200 nM conjugate dispersions. Similarly, greater intracellular staining was measured for cells incubated with QD-FA conjugates for longer times (see Figure 8C), indicating that the uptake is also time-dependent. Taken together, these results prove that the folic acid-modified polymer ligand promotes specific cellular internalization of QDs in a concentration- and time-dependent manner.

**Cellular Uptake of QD–Transferrin Conjugates.** Here we tested the intracellular uptake of QDs conjugated to the protein receptor transferrin after phase transfer to buffer. For this, we started with QDs capped with His-PIMA-ZW ligands. The carboxylic acid groups along the PIMA backbone were then activated with EDC/NHS, followed by reaction with lysine amino acids of transferrin (via carboxyl-to-amine cross-linking),<sup>79</sup> as illustrated in Figure 9A. The QD–transferrin conjugates were separated from byproducts using a PD-10 size-exclusion column and then incubated with HeLa cells at 200 nM for 1 h. These cells were washed twice with phosphate-buffered saline (PBS) and subsequently incubated with 0.5  $\mu$ M Texas Red–transferrin (as an endosome marker) for an additional 40 min. Figure 9B shows that the green signal of the QDs was observed for the cells incubated with QD–transferrin and that the distribution was fully colocalized with that of the Texas Red–transferrin marker, indicating that here too the uptake occurred via endocytosis. Control experiments indicated that incubation of cells with unconjugated QDs at the same concentration resulted in no intracellular signal (data not shown).

Taken together, these findings indicate that the prepared polymer-coated QDs can be reacted post phase transfer with specific proteins or peptides via either metal–polyhistidine conjugation or covalent coupling to yield bioreactive conjugates. Alternatively, biomolecules can be introduced into the polymer structure in situ during the ligand synthesis prior to ligand exchange on the nanocrystal. The conjugates prepared via either

route can be effectively used in applications such as sensing, cellular uptake, and imaging.

We would like to provide a contextual comparison between the PEG-based polymer ligands reported in ref 39 (i.e., LA/His-PIMA-PEG) and the ones prepared and tested in this report (i.e., His-PIMA-ZW). Even though the chemical designs to prepare the ligands are similar, relying on the efficient nucleophilic addition reaction starting from poly(isobutylene-*alt*-maleic anhydride), there are a few key differences that influence the QD behavior in buffer media. The present ligand design takes advantage of the effective anhydride reactivity toward amine-presenting molecules but substitutes zwitterion moieties for short PEG chains and uses only imidazole anchors for coordination to the QD surface. This yields QDs with high PL yields in buffer media (comparable to those measured for hydrophobic QDs) and, more importantly, very compact overall dimensions. The  $R_H$  value measured here is comparable to that measured for DHLA-QDs, which is remarkable for a polymer coating strategy. The coating yields a net negative charge density, resulting from the contribution of the carboxyl groups freed during the reaction and the newly introduced sulfobetaine groups; these groups tend to stay negatively charged even in acidic buffers. The similar mobilities of the QD dispersions over the pH range 5–13 (Figure 3C) indicates that there are no pH effects on the overall charge distribution of His-PIMA-ZW-QDs. Finally, the use of only imidazole coordination combined with zwitterion moieties provides nanocrystals that are fully compatible with metal–histidine self-assembly of polyhistidine-tagged full-sized proteins on the QDs. This is very promising for potential use in biology. Nonetheless, the absence of lipoic acid anchors from the His-PIMA-ZW ligands provides less optimal colloidal stability under acidic conditions, consistent with the PEGylated polymer with imidazole anchors only (i.e., His-PIMA-PEG).

## CONCLUSION

We have developed a new set of metal-coordinating polymer ligands combining the imidazole anchoring group with the hydrophilic zwitterion motif and used them for the surface functionalization of luminescent QDs. The ligand design exploits the highly efficient nucleophilic addition reaction between poly(isobutylene-*alt*-maleic anhydride) (PIMA) and amines and was used to introduce a controllable number of imidazole anchors, hydrophilic zwitterion moieties, and reactive groups on the same polymer chain. We have further exploited this addition reaction to introduce biomolecules (such as folic acid as a cancer-cell-targeting agent) into the polymer ligands prior to ligation to the QDs. This expands on our previous work using the PIMA precursor to prepare other PEG-based ligands; those ligands were used to functionalize iron oxide nanoparticles, QDs, and AuNPs.<sup>39,55,80</sup>

Ligation with these polymers yields hydrophilic QDs that exhibit excellent colloidal stability over a broad range of biological conditions, including storage at very low concentrations and under ambient conditions and a resistance against chemical oxidation by H<sub>2</sub>O<sub>2</sub>. This very thin hydrophilic coating afforded by the zwitterion motif yields QDs with a small hydrodynamic radius ( $R_H \approx 5$ –6 nm), allowing conjugation with polyhistidine-tagged proteins via metal-affinity coordination. We have also shown that coupling of dopamine onto the QDs provides fluorescent platforms that can sense changes in pH of the medium, the presence of Fe ions, and interactions with cysteine. Finally, we have found that ligating QDs with the



folic acid-modified polymer can promote the effective delivery of large amounts of QDs into living cancer cells via folate-receptor-mediated endocytosis.

These results are greatly promising for fluorescent labeling in biology, including cellular imaging and sensing, where probes that are small in size and stable at very low concentrations are often required. Conjugates prepared with such nanocrystals would find great use in imaging of blood vasculature and tracking of protein migration in live cells and tissues. We also anticipate that this chemical design will be applicable to the preparation of additional polymers with other functionalities adapted to different inorganic nanocrystals. This nucleophilic addition reaction can be easily used to develop various functional polymers with potential applications in antifouling coatings and for chelation to transition metal surfaces.

## EXPERIMENTAL SECTION

**Synthesis of His-PIMA-ZW.** In a 50 mL three-neck round-bottom flask equipped with an addition funnel and a magnetic stirring bar, 0.385 g of PIMA (MW  $\approx$  6000 g/mol, 2.5 mmol of monomer units) was dissolved in 5 mL of DMSO. The solution was purged with nitrogen for 10 min and then heated to 45 °C. Histamine (0.139 g, 1.25 mmol) was dissolved in 1 mL of DMSO using a scintillation vial, and this solution was added dropwise to the PIMA solution through the addition funnel. After that, 1 mL of DMSO solution containing ZW-NH<sub>2</sub> (0.280 g, 1.25 mmol) was added, and the reaction mixture was left to stir at 45 °C overnight. The solution was concentrated to  $\sim$ 2 mL under vacuum, and a large excess of acetone was added to precipitate the compound, followed by centrifugation. The solid pellet was washed three times with acetone and then dried under vacuum, providing the final product as white powder; the reaction yield was  $\sim$ 93%.

**Synthesis of His-PIMA-ZW/NH<sub>2</sub> (10% Amine).** PIMA (0.385 g, 2.5 mmol of monomers) was dissolved in 5 mL of dry DMSO using a 50 mL round-bottom flask equipped with an addition funnel and a magnetic stirring bar. The solution was purged with nitrogen for 10 min and then heated to 45 °C. To the stirring solution, 1 mL of DMSO containing histamine (0.139 g, 1.25 mmol) was added dropwise through the addition funnel, followed by 1 mL of DMSO containing ZW-NH<sub>2</sub> (0.224 g, 1 mmol). After 2 h, H<sub>2</sub>N-PEG-NH<sub>2</sub> (0.15 g, 0.25 mmol) dissolved in 1 mL of DMSO was finally added to the reaction mixture. Once the addition was complete, the mixture was stirred at 45 °C overnight. The solvent was then removed under vacuum, and the compound was precipitated by the addition of a large excess of acetone. After centrifugation, the solid pellet was washed with acetone and dried under vacuum. The final compound was obtained as a yellowish solid in a reaction yield of  $\sim$ 85%.

**Synthesis of His-PIMA-ZW/FA (10% Folic Acid).** In 50 mL three-neck round-bottom flask equipped with a magnetic stirring bar, PIMA (0.15 g, 0.975 mmol of monomers) was dissolved in 3 mL of DMSO, and then the solution was purged with nitrogen for 10 min while stirring. To this solution, 1 mL of DMSO containing histamine (0.0542 g, 0.487 mmol) was added dropwise using a syringe. This was followed by the stepwise addition of 1 mL of folic acid solution in DMSO (0.043 g, 0.097 mmol) and 1 mL of DMSO containing ZW-NH<sub>2</sub> (0.087 g, 0.39 mmol). The reaction mixture was further stirred at room temperature overnight and then concentrated to  $\sim$ 1 mL under vacuum. The compound was precipitated by the addition of excess acetone and centrifuged for 3 min at 3700 rpm. The resulting solid pellet was washed with acetone and dried under vacuum, yielding a yellow powder; the reaction yield was  $\sim$ 86%.

**Synthesis of the QDs.** The nanocrystals used in this study were made of CdSe–ZnS core–shell QDs grown via reduction of organometallic precursors at high temperature in a hot coordinating solvent mixture in two steps: growth of the CdSe core followed by ZnS overcoating. The growth of the CdSe core involved the reduction of cadmium and selenium precursors at high temperature in a hot (300–350 °C) coordinating solvent mixture made of TOP, TOPO, alkylamines, and alkylcarboxyls; the nanocrystal core size was

controlled by adjusting the precursor concentrations and temperature. Overcoating of the CdSe core with a ZnS shell using zinc was carried out at lower temperature. The QD sizes were tuned by varying the CdSe core radius while maintaining the same thickness of the overcoating ZnS layer. A detailed description of the QD growth (both core and shell) is provided in the [Supporting Information](#).

**Ligand Exchange.** We limit our description to the preparation of QDs capped with His-PIMA-ZW; the same protocol is applicable to capping with the other ligands. A solution of hydrophobic QDs (26.7  $\mu$ M, 150  $\mu$ L) was precipitated using ethanol and redispersed in 200  $\mu$ L of chloroform. Separately, 15 mg of His-PIMA-ZW was dissolved in 200  $\mu$ L of DMSO with gentle heating and sonication (for  $\sim$ 3–5 min). The ligand solution and the QD dispersion were then mixed in a scintillation vial. The vial was sealed with a rubber septum, and the atmosphere was switched to nitrogen by applying two or three rounds of mild vacuum followed by purging with nitrogen; the mixture was then left to stir at room temperature overnight. The QDs were precipitated by the addition of 500  $\mu$ L of hexane and acetone (in excess). Following sonication for  $\sim$ 1 min, the solution was centrifuged at 3700 rpm for  $\sim$ 5 min, yielding a pellet. The procedure was repeated one more time. The final precipitate was dried under vacuum for  $\sim$ 10 min to yield a powder, which could then be readily dispersed in 3–5 mL of phosphate buffer (pH 12, 50 mM); sonication for  $\sim$ 5 min was needed to fully disperse the powder in some cases. The obtained clear aqueous dispersion of QDs was filtered through a 0.45  $\mu$ M syringe filter, and excess free ligands were removed by applying 3–4 rounds of concentration/dilution with DI water using a centrifugal filtration device (MW cutoff = 50 kDa; Millipore). This protocol provided clear QD dispersions, e.g.,  $\sim$ 500  $\mu$ L with a concentration of  $\sim$ 7–8  $\mu$ M. Ligand exchange with His-PIMA-ZW/NH<sub>2</sub> or His-PIMA-ZW/FA was carried out following the same steps, except that the amount of polymer ligand used was  $\sim$ 20 mg in each case.

*Remark:* When the ligand solution was mixed with the QD dispersion in an organic mixture, the solution progressively became turbid because of the limited solubility of zwitterion moieties in the polymer coating.

**NMR Sample Preparation.** We used pulsed-field-gradient water suppression to collect the <sup>1</sup>H NMR spectra. Briefly, after ligand exchange and phase transfer of the QDs (as described above), the DI water was switched to D<sub>2</sub>O by applying two rounds of concentration/dilution using deuterium oxide (2 mL each). The final volume of the QD dispersions in D<sub>2</sub>O used to collect the NMR spectra was adjusted to 500  $\mu$ L, and the concentration was  $\sim$ 8–9  $\mu$ M. The <sup>1</sup>H NMR spectra were collected by averaging over 500 scans. The same sample was used to collect the <sup>31</sup>P NMR spectrum of His-PIMA-ZW-QDs in D<sub>2</sub>O. The <sup>31</sup>P NMR spectrum of the hydrophobic QDs was collected using nanocrystals prepared from the stock dispersion, via one round of precipitation with excess ethanol, drying under vacuum and redispersion in CDCl<sub>3</sub>. The concentration was  $\sim$ 10  $\mu$ M.

The samples used for surface-ligand counting experiments were prepared following the same protocol, but 2  $\mu$ L of pyridine (24.8  $\mu$ mol) dissolved in 5  $\mu$ L of D<sub>2</sub>O was added to the QD dispersion as a standard. We should note that the final QD concentration in the NMR sample was slightly altered with the addition of pyridine (e.g., addition of pyridine reduced the QD concentration from  $\sim$ 8.6 to  $\sim$ 8.5  $\mu$ M).

**Assembly of QD–Protein Conjugates.** Two different proteins were used for conjugation to the QDs via metal–histidine-promoted self-assembly: maltose binding protein appended with a seven-histidine sequence (MBP-His<sub>7</sub>) and the fluorescent mCherry protein appended with a six-histidine sequence (mCherry-His<sub>6</sub>); both sequences were inserted at the N-terminus.<sup>63</sup> The protein expression and purification, briefly summarized in the [Supporting Information](#), were carried out following the protocols detailed in ref 63. The conjugation was carried out using the same steps for both proteins. Here we detail the assembly of QD–mCherry conjugates with varying valence. Approximately 22.2  $\mu$ L aliquots of a stock QD dispersion (3.6  $\mu$ M) were loaded into Eppendorf tubes, and the volume in each tube was adjusted to 100  $\mu$ L by addition of phosphate buffer (pH 8.0, 40 mM). The desired amounts of mCherry solutions were loaded into separate tubes, followed by the addition of phosphate buffer to bring the total volume to 300  $\mu$ L. The



mCherry:QD ratio (i.e., the valence) was varied from 0.5:1 to 12:1. For example, a dispersion with a valence of  $\sim 1$  was prepared by addition of  $\sim 6.2 \mu\text{L}$  of mCherry stock solution ( $12.9 \mu\text{M}$ ) to  $294 \mu\text{L}$  of phosphate buffer followed by gentle mixing with the QD dispersion and incubation at  $4^\circ\text{C}$  for 30 min to allow for self-assembly. The samples were then characterized by collecting the absorption and emission spectra.

**QD–Dopamine Conjugates.** Freshly prepared QDs capped with His-PIMA-ZW/ $\text{NH}_2$  (10% amine) were reacted with dopamine-ITC to provide the final QD–dopamine conjugates.<sup>70</sup> We prepared three sets of conjugate dispersions by reacting the His-PIMA-ZW/ $\text{NH}_2$ -QDs with different amounts of dopamine-ITC. The first set was prepared by addition of  $25 \mu\text{L}$  aliquots of dopamine-ITC predissolved in DMSO ( $0.5 \text{ mg/mL}$ ) to scintillation vials containing  $136 \mu\text{L}$  of QD dispersion ( $\sim 5.90 \mu\text{M}$ ) and  $20 \mu\text{L}$  of NaCl solution ( $1 \text{ M}$ ); DI water was then added to bring the total volume to  $\sim 1 \text{ mL}$ . The mixtures were then stirred for  $\sim 3 \text{ h}$  in the dark, followed by removal of excess free/unreacted dopamine using one round of concentration/dilution through a membrane filtration device (MW cutoff =  $50 \text{ kDa}$ ; Millipore) to provide the final conjugate dispersions ( $1 \text{ mL}$  and  $\sim 0.8 \mu\text{M}$  QD concentration). For the other two samples,  $50$  and  $100 \mu\text{L}$  aliquots of dopamine-ITC were reacted with the QD dispersions.

1. **pH-Dependent Quenching of QD Fluorescence.** The pH-dependent PL quenching data were collected for all three sets of conjugates with a QD–dopamine concentration of  $\sim 32 \text{ nM}$ . These were prepared by mixing  $40 \mu\text{L}$  aliquots of the conjugate stock dispersions with  $960 \mu\text{L}$  of phosphate buffer ( $10 \text{ mM}$ ) at the desired pH. The fluorescence spectra were collected for each sample, and the integrated PL signal was reported relative to the value measured at pH 4.

2. **Interactions of QD–Dopamine Conjugates with Soluble Cysteine.** The stock dispersions of QD–dopamine conjugates used in these experiments were prepared using  $50 \mu\text{L}$  of dopamine-ITC (intermediate dopamine valence). First,  $40 \mu\text{L}$  aliquots of the QD–dopamine conjugates were dispersed in phosphate buffer (pH 10,  $10 \text{ mM}$ ), and then the desired volumes of cysteine stock solution (concentration =  $0.1 \text{ mM}$ ) were added. The volumes of the solutions were adjusted to a final value of  $1 \text{ mL}$  by addition of the required amounts of pH 10 buffer. The cysteine concentrations used in these measurements were  $1$ ,  $4$ , and  $8 \mu\text{M}$  (i.e., excess cysteine). The mixtures were incubated for different time periods, and the PL spectra were recorded after each period.

3. **Fluorescence Sensing of Fe Ions Using QD–Dopamine Conjugates.** Here we started with the dispersions of QD–dopamine conjugates having the lowest valence (dispersions of conjugates prepared using  $25 \mu\text{L}$  of dopamine-ITC). The conditions used for conjugation of QDs to dopamine-ITC were identical to those described above, except that the DI water was purged with argon for  $\sim 20 \text{ min}$ .<sup>70</sup> Separately, a stock solution of Fe ion ( $2 \text{ mM}$ ) was freshly prepared by dissolving  $\text{FeCl}_3 \cdot 6\text{H}_2\text{O}$  in DI water. Then  $50 \mu\text{L}$  aliquots of the QD–dopamine dispersions were diluted in DI water and mixed with the desired volumes of Fe solution. The final total volume of each mixture was  $1.5 \text{ mL}$ . The concentration of QD–dopamine conjugates was fixed at  $\sim 26.7 \text{ nM}$ , while that of Fe ions was varied from  $0$  to  $20 \mu\text{M}$ . The PL spectrum of each dispersion was collected, and the intensity was plotted versus the Fe ion concentration.

4. **Cysteine-Induced PL Recovery of QD–Dopamine–Fe Complex Conjugates.** We started with a dispersion of QD–dopamine premixed with Fe ions (i.e., with quenched QD PL). This dispersion was prepared by dilution of  $50 \mu\text{L}$  of QD–dopamine conjugates in  $1.423 \text{ mL}$  of DI water followed by the addition of  $15 \mu\text{L}$  of Fe solution ( $2 \text{ mM}$ ). Then  $12 \mu\text{L}$  of cysteine was added to the above solution, and the resulting solution was mixed. The final total volume of the dispersion was  $1.5 \text{ mL}$ , while the final concentrations of Fe and cysteine were  $20$  and  $8 \mu\text{M}$ , respectively. The PL spectra of the sample were recorded at different time intervals. We started with the Fe concentration that gave us the highest quenching (see Results and Discussion).

**Preparation of QD–Transferrin Conjugates.** To prepare the QD–transferrin conjugates, the carboxylic groups available on the His-PIMA-ZW-QDs (freed during the addition reaction) were reacted with

the amine groups of transferrin via the EDC/NHS condensation reaction.<sup>79</sup> Briefly,  $50 \mu\text{L}$  of His-PIMA-ZW-capped QDs ( $7.22 \mu\text{M}$ ) was first dispersed in  $400 \mu\text{L}$  of phosphate buffer (pH 6.5,  $50 \text{ mM}$ ), and then a 100-fold excess of NHS ( $8.5 \text{ mM}$ ,  $4.2 \mu\text{L}$ ) and EDC ( $5 \text{ mM}$ ,  $7.2 \mu\text{L}$ ) dissolved in DI water was added. The reaction was left to proceed for  $\sim 3 \text{ h}$  at room temperature, and then the excess EDC and NHS were removed by applying one round of dilution/concentration with DI water using a membrane filtration device (MW cutoff =  $50 \text{ kDa}$ ; Millipore). The purified QD–NHS esters were added to  $400 \mu\text{L}$  of phosphate buffer (pH 7.8,  $20 \text{ mM}$ ) containing  $\sim 20$ -fold excess of transferrin ( $0.58 \text{ mg}$ , MW =  $80 \text{ kDa}$ ) with respect to the QD concentration, and the mixture was incubated at  $4^\circ\text{C}$  overnight. The conjugates were separated from unbound transferrin and NHS byproducts via size-exclusion chromatography using a PD 10 column. The first eluted fraction containing the QD–transferrin conjugates was used for the cellular uptake experiments.

**Cell Imaging.** HeLa cell cultures (human cervix carcinoma cell line), provided by the Florida State University cell culture facility, were grown at  $37^\circ\text{C}$  in a humidified 5%  $\text{CO}_2$  atmosphere at  $37^\circ\text{C}$  as a monolayer in a complete growth medium (Dulbecco's Modified Eagle's Medium (DMEM), Cellgro) supplemented with 10% (v/v) fetal bovine serum (Gibco),  $4.5 \text{ g/L}$  glucose, L-glutamine, sodium pyruvate, 1% (v/v) antibiotic-antimycotic  $100\times$  (Gibco), and 1% (v/v) nonessential amino acid solution  $100\times$  (Sigma). Then  $8 \times 10^4$  of the above cells were seeded onto  $12 \text{ mm}$  round microcover glasses in a 24-well microplate (CellStar, VWR). The plates were placed in an incubator for  $24 \text{ h}$  to allow for cell attachment. The cells were then incubated with QD–FA or QD–transferrin conjugates and Texas Red-labeled transferrin (at a concentration of  $\sim 0.5 \mu\text{M}$ ). The QD concentrations and incubation times were adjusted according to the experimental needs. After incubation, the cells were washed twice with PBS buffer, fixed with 3.7% paraformaldehyde, and stained with DAPI (Prolong Antifade mounting medium with DAPI nuclear staining, Invitrogen). Control experiments were carried out by incubating the cells with polymer-coated QDs without folic acid or transferrin. The fluorescence images were acquired using an Inverted Nikon Eclipse Ti Microscope equipped with a color CoolSNAP HQ2 CCD camera. Excitation of the sample was provided by a Xe lamp, while the fluorescence images were collected using a  $60\times$  objective (Nikon) and a set of filter cubes (Chroma Technology, Rockingham, VT). The DAPI fluorescence was detected using a DAPI cube (with  $340$ – $380 \text{ nm}$  excitation and  $435$ – $485 \text{ nm}$  emission), the QD signal was detected using a GFP/EGFP cube (with  $450$ – $490 \text{ nm}$  excitation and  $500$ – $550 \text{ nm}$  emission), and the Texas Red–transferrin fluorescence was detected using a TEXAS RED HYQ cube (with  $532$ – $587 \text{ nm}$  excitation and  $608$ – $683 \text{ nm}$  emission).

## ■ ASSOCIATED CONTENT

### Supporting Information

The Supporting Information is available free of charge on the ACS Publications website at DOI: [10.1021/jacs.5b08915](https://doi.org/10.1021/jacs.5b08915).

Materials, instrumentation, additional experimental details, synthesis of amino-zwitterion,  $^1\text{H}$  NMR characterization of ZW- $\text{NH}_2$ , optical characterization of additional His-PIMA-ZW-capped QDs,  $^{31}\text{P}$  spectra of QDs capped with TOP/TOPO/HPA and His-PIMA-ZW, additional  $^1\text{H}$  NMR spectra of His-PIMA-ZW/FA-QDs and His-PIMA-ZW-QDs, FRET analysis, control experiments for sensing cysteine and iron ions, and control experiment on cellular uptake of QDs alone (PDF)

## ■ AUTHOR INFORMATION

### Corresponding Author

\*[mattoussi@chem.fsu.edu](mailto:mattoussi@chem.fsu.edu)

### Notes

The authors declare no competing financial interest.

## ACKNOWLEDGMENTS

The authors thank Florida State University and the National Science Foundation for financial support (NSF CHE 1508501 and 1058957).

## REFERENCES

- (1) Murray, C. B.; Norris, D. J.; Bawendi, M. G. *J. Am. Chem. Soc.* **1993**, *115*, 8706.
- (2) Alivisatos, A. P. *J. Phys. Chem.* **1996**, *100*, 13226.
- (3) Murray, C. B.; Kagan, C. R.; Bawendi, M. G. *Annu. Rev. Mater. Sci.* **2000**, *30*, 545.
- (4) Peng, Z. A.; Peng, X. G. *J. Am. Chem. Soc.* **2001**, *123*, 183.
- (5) Talapin, D. V.; Rogach, A. L.; Kornowski, A.; Haase, M.; Weller, H. *Nano Lett.* **2001**, *1*, 207.
- (6) Hines, M. A.; Guyot-Sionnest, P. *J. Phys. Chem.* **1996**, *100*, 468.
- (7) Dabbousi, B. O.; RodriguezViejo, J.; Mikulec, F. V.; Heine, J. R.; Mattoussi, H.; Ober, R.; Jensen, K. F.; Bawendi, M. G. *J. Phys. Chem. B* **1997**, *101*, 9463.
- (8) Reiss, P.; Bleuse, J.; Pron, A. *Nano Lett.* **2002**, *2*, 781.
- (9) Wu, X. Y.; Liu, H. J.; Liu, J. Q.; Haley, K. N.; Treadway, J. A.; Larson, J. P.; Ge, N. F.; Peale, F.; Bruchez, M. P. *Nat. Biotechnol.* **2003**, *21*, 41.
- (10) Michalet, X.; Pinaud, F.; Bentolila, L.; Tsay, J.; Doose, S.; Li, J.; Sundaresan, G.; Wu, A.; Gambhir, S.; Weiss, S. *Science* **2005**, *307*, 538.
- (11) Zrazhevskiy, P.; Sena, M.; Gao, X. H. *Chem. Soc. Rev.* **2010**, *39*, 4326.
- (12) Chou, L. Y. T.; Ming, K.; Chan, W. C. W. *Chem. Soc. Rev.* **2011**, *40*, 233.
- (13) Freeman, R.; Willner, I. *Chem. Soc. Rev.* **2012**, *41*, 4067.
- (14) Kairdolf, B. A.; Smith, A. M.; Stokes, T. H.; Wang, M. D.; Young, A. N.; Nie, S. M. *Annu. Rev. Anal. Chem.* **2013**, *6*, 143.
- (15) Kim, C. S.; Duncan, B.; Creran, B.; Rotello, V. M. *Nano Today* **2013**, *8*, 439.
- (16) Sapsford, K. E.; Algar, W. R.; Berti, L.; Gemmill, K. B.; Casey, B. J.; Oh, E.; Stewart, M. H.; Medintz, I. L. *Chem. Rev.* **2013**, *113*, 1904.
- (17) Howes, P. D.; Chandrawati, R.; Stevens, M. M. *Science* **2014**, *346*, 1247390.
- (18) Lemon, C. M.; Curtin, P. N.; Somers, R. C.; Greytak, A. B.; Lanning, R. M.; Jain, R. K.; Bawendi, M. G.; Nocera, D. G. *Inorg. Chem.* **2014**, *53*, 1900.
- (19) Palui, G.; Aldeek, F.; Wang, W.; Mattoussi, H. *Chem. Soc. Rev.* **2015**, *44*, 193.
- (20) Silvi, S.; Credi, A. *Chem. Soc. Rev.* **2015**, *44*, 4275.
- (21) Choi, H. S.; Liu, W.; Misra, P.; Tanaka, E.; Zimmer, J. P.; Ipe, B. I.; Bawendi, M. G.; Frangioni, J. V. *Nat. Biotechnol.* **2007**, *25*, 1165.
- (22) Baker, M. *Nat. Methods* **2010**, *7*, 957.
- (23) Liu, W. H.; Greytak, A. B.; Lee, J.; Wong, C. R.; Park, J.; Marshall, L. F.; Jiang, W.; Curtin, P. N.; Ting, A. Y.; Nocera, D. G.; Fukumura, D.; Jain, R. K.; Bawendi, M. G. *J. Am. Chem. Soc.* **2010**, *132*, 472.
- (24) Giovanelli, E.; Muro, E.; Sitbon, G.; Hanafi, M.; Pons, T.; Dubertret, B.; Lequeux, N. *Langmuir* **2012**, *28*, 15177.
- (25) Han, H. S.; Martin, J. D.; Lee, J.; Harris, D. K.; Fukumura, D.; Jain, R. K.; Bawendi, M. *Angew. Chem., Int. Ed.* **2013**, *52*, 1414.
- (26) Cai, E.; Ge, P.; Lee, S. H.; Jeyifous, O.; Wang, Y.; Liu, Y.; Wilson, K. M.; Lim, S. J.; Baird, M. A.; Stone, J. E.; Lee, K. Y.; Davidson, M. W.; Chung, H. J.; Schulten, K.; Smith, A. M.; Green, W. N.; Selvin, P. R. *Angew. Chem., Int. Ed.* **2014**, *53*, 12484.
- (27) Mattoussi, H.; Palui, G.; Na, H. B. *Adv. Drug Delivery Rev.* **2012**, *64*, 138.
- (28) Dahan, M.; Levi, S.; Luccardini, C.; Rostaing, P.; Riveau, B.; Triller, A. *Science* **2003**, *302*, 442.
- (29) Dubertret, B.; Skourides, P.; Norris, D. J.; Noireaux, V.; Brivanlou, A. H.; Libchaber, A. *Science* **2002**, *298*, 1759.
- (30) Susumu, K.; Uyeda, H. T.; Medintz, I. L.; Pons, T.; Delehanty, J. B.; Mattoussi, H. *J. Am. Chem. Soc.* **2007**, *129*, 13987.
- (31) Yu, W. W.; Chang, E.; Falkner, J. C.; Zhang, J. Y.; Al-Somali, A. M.; Sayes, C. M.; Johns, J.; Drezek, R.; Colvin, V. L. *J. Am. Chem. Soc.* **2007**, *129*, 2871.
- (32) Liu, W.; Howarth, M.; Greytak, A. B.; Zheng, Y.; Nocera, D. G.; Ting, A. Y.; Bawendi, M. G. *J. Am. Chem. Soc.* **2008**, *130*, 1274.
- (33) Yildiz, I.; McCaughan, B.; Cruickshank, S. F.; Callan, J. F.; Raymo, F. M. *Langmuir* **2009**, *25*, 7090.
- (34) Lees, E. E.; Nguyen, T. L.; Clayton, A. H. A.; Mulvaney, P. *ACS Nano* **2009**, *3*, 1121.
- (35) Lin, C. A. J.; Sperling, R. A.; Li, J. K.; Yang, T. Y.; Li, P. Y.; Zanella, M.; Chang, W. H.; Parak, W. G. *J. Small* **2008**, *4*, 334.
- (36) Thiry, M.; Boldt, K.; Nikolic, M. S.; Schulz, F.; Ijeh, M.; Panicker, A.; Vossmeier, T.; Weller, H. *ACS Nano* **2011**, *5*, 4965.
- (37) Zhang, F.; Lees, E.; Amin, F.; Rivera-Gil, P.; Yang, F.; Mulvaney, P.; Parak, W. *J. Small* **2011**, *7*, 3113.
- (38) Nagaraja, A. T.; Soorash, A.; Meissner, K. E.; McShane, M. J. *ACS Nano* **2013**, *7*, 6194.
- (39) Wang, W.; Kapur, A.; Ji, X.; Safi, M.; Palui, G.; Palomo, V.; Dawson, P. E.; Mattoussi, H. *J. Am. Chem. Soc.* **2015**, *137*, 5438.
- (40) Bullen, C.; Mulvaney, P. *Langmuir* **2006**, *22*, 3007.
- (41) Mattoussi, H.; Cheon, J. *Inorganic Nanoprobes for Biological Sensing and Imaging*; Artech House: Boston, 2009.
- (42) Muro, E.; Pons, T.; Lequeux, N.; Fragola, A.; Sanson, N.; Lenkei, Z.; Dubertret, B. *J. Am. Chem. Soc.* **2010**, *132*, 4556.
- (43) Park, J.; Nam, J.; Won, N.; Jin, H.; Jung, S.; Cho, S. H.; Kim, S. *Adv. Funct. Mater.* **2011**, *21*, 1558.
- (44) Zhan, N. Q.; Palui, G.; Safi, M.; Ji, X.; Mattoussi, H. *J. Am. Chem. Soc.* **2013**, *135*, 13786.
- (45) Sun, M. H.; Yang, L. K.; Jose, P.; Wang, L.; Zweit, J. *J. Mater. Chem. B* **2013**, *1*, 6137.
- (46) Garcia, K. P.; Zarschler, K.; Barbaro, L.; Barreto, J. A.; O'Malley, W.; Spiccia, L.; Stephan, H.; Graham, B. *Small* **2014**, *10*, 2516.
- (47) Susumu, K.; Oh, E.; Delehanty, J. B.; Blanco-Canosa, J. B.; Johnson, B. J.; Jain, V.; Hervey, W. J.; Algar, W. R.; Boeneman, K.; Dawson, P. E.; Medintz, I. L. *J. Am. Chem. Soc.* **2011**, *133*, 9480.
- (48) Zhang, P.; Liu, S.; Gao, D.; Hu, D.; Gong, P.; Sheng, Z.; Deng, J.; Ma, Y.; Cai, L. *J. Am. Chem. Soc.* **2012**, *134*, 8388.
- (49) Viswanath, A.; Shen, Y.; Green, A. N.; Tan, R.; Greytak, A. B.; Benicewicz, B. C. *Macromolecules* **2014**, *47*, 8137.
- (50) Ghadiali, J. E.; Cohen, B. E.; Stevens, M. M. *ACS Nano* **2010**, *4*, 4915.
- (51) Mattoussi, H.; Mauro, J. M.; Goldman, E. R.; Anderson, G. P.; Sundar, V. C.; Mikulec, F. V.; Bawendi, M. G. *J. Am. Chem. Soc.* **2000**, *122*, 12142.
- (52) Medintz, I. L.; Clapp, A. R.; Mattoussi, H.; Goldman, E. R.; Fisher, B.; Mauro, J. M. *Nat. Mater.* **2003**, *2*, 630.
- (53) Clapp, A. R.; Medintz, I. L.; Mauro, J. M.; Fisher, B. R.; Bawendi, M. G.; Mattoussi, H. *J. Am. Chem. Soc.* **2004**, *126*, 301.
- (54) Dif, A.; Boulmedais, F.; Pinot, M.; Roullier, V.; Baudy-Floc'h, M.; Coquelle, F. M.; Clarke, S.; Neveu, P.; Vignaux, F.; Le Borgne, R.; Dahan, M.; Gueroui, Z.; Marchi-Artzner, V. *J. Am. Chem. Soc.* **2009**, *131*, 14738.
- (55) Wang, W.; Ji, X.; Na, H. B.; Safi, M.; Smith, A.; Palui, G.; Perez, J. M.; Mattoussi, H. *Langmuir* **2014**, *30*, 6197.
- (56) Susumu, K.; Mei, B. C.; Mattoussi, H. *Nat. Protoc.* **2009**, *4*, 424.
- (57) Hens, Z.; Martins, J. C. *Chem. Mater.* **2013**, *25*, 1211.
- (58) Einstein, A. *Ann. Phys.* **1905**, *322*, 549.
- (59) Edward, J. T. *J. Chem. Educ.* **1970**, *47*, 261.
- (60) Pons, T.; Uyeda, H. T.; Medintz, I. L.; Mattoussi, H. *J. Phys. Chem. B* **2006**, *110*, 20308.
- (61) Mattoussi, H.; Cumming, A. W.; Murray, C. B.; Bawendi, M. G.; Ober, R. *Phys. Rev. B: Condens. Matter Mater. Phys.* **1998**, *58*, 7850.
- (62) Paiva, T. B.; Tominaga, M.; Paiva, A. C. M. *J. Med. Chem.* **1970**, *13*, 689.
- (63) Aldeek, F.; Safi, M.; Zhan, N. Q.; Palui, G.; Mattoussi, H. *ACS Nano* **2013**, *7*, 10197.
- (64) Medintz, I. L.; Pons, T.; Susumu, K.; Boeneman, K.; Dennis, A. M.; Farrell, D.; Deschamps, J. R.; Melinger, J. S.; Bao, G.; Mattoussi, H. *J. Phys. Chem. C* **2009**, *113*, 18552.
- (65) LaVoie, M. J.; Ostaszewski, B. L.; Weihofen, A.; Schlossmacher, M. G.; Selkoe, D. J. *Nat. Med.* **2005**, *11*, 1214.
- (66) Olanow, C. W.; Tatton, W. G. *Annu. Rev. Neurosci.* **1999**, *22*, 123.

- (67) Jiang, D.; Shi, S.; Zhang, L.; Liu, L.; Ding, B.; Zhao, B.; Yagnik, G.; Zhou, F. *ACS Chem. Neurosci.* **2013**, *4*, 1305.
- (68) Mosca, L.; Lendaro, E.; d'Erme, M.; Marcellini, S.; Moretti, S.; Rosei, M. A. *Neurochem. Int.* **2006**, *49*, 262.
- (69) Sulzer, D.; Bogulavsky, J.; Larsen, K. E.; Behr, G.; Karatekin, E.; Kleinman, M. H.; Turro, N.; Krantz, D.; Edwards, R. H.; Greene, L. A.; Zecca, L. *Proc. Natl. Acad. Sci. U. S. A.* **2000**, *97*, 11869.
- (70) Ji, X.; Palui, G.; Avellini, T.; Na, H. B.; Yi, C.; Knappenberger, K. L.; Mattoussi, H. *J. Am. Chem. Soc.* **2012**, *134*, 6006.
- (71) Ji, X.; Wang, W.; Mattoussi, H. *Phys. Chem. Chem. Phys.* **2015**, *17*, 10108.
- (72) Ji, X.; Makarov, N. S.; Wang, W.; Palui, G.; Robel, I.; Mattoussi, H. *J. Phys. Chem. C* **2015**, *119*, 3388.
- (73) Low, P. S.; Henne, W. A.; Doorneweerd, D. D. *Acc. Chem. Res.* **2008**, *41*, 120.
- (74) Campbell, I. G.; Jones, T. A.; Foulkes, W. D.; Trowsdale, J. *Cancer Res.* **1991**, *51*, 5329.
- (75) Lee, R. J.; Low, P. S. *J. Biol. Chem.* **1994**, *269*, 3198.
- (76) Kamen, B. A.; Capdevila, A. *Proc. Natl. Acad. Sci. U. S. A.* **1986**, *83*, 5983.
- (77) Bharali, D. J.; Lucey, D. W.; Jayakumar, H.; Pudavar, H. E.; Prasad, P. N. *J. Am. Chem. Soc.* **2005**, *127*, 11364.
- (78) Lu, Y. J.; Low, P. S. *Adv. Drug Delivery Rev.* **2002**, *54*, 675.
- (79) Hermanson, G. T. *Bioconjugate Techniques*, 3rd ed.; Academic Press: London, 2013; p 1.
- (80) Wang, W.; Aldeek, F.; Ji, X.; Zeng, B. R.; Mattoussi, H. *Faraday Discuss.* **2014**, *175*, 137.